Title

LC3 Binding to the Scaffolding Protein JIP1 Regulates Processive Dynein-Driven Transport of Autophagosomes

Journal

Developmental Cell, 29(5)

ISSN

1534-5807

Authors

Fu, Meng-meng
Nirschl, Jeffrey J
Holzbaur, Erika LF

Publication Date

2014-06-01

DOI

10.1016/j.devcel.2014.04.015

Peer reviewed

Published in final edited form as:
Dev Cell. 2014 June 9; 29(5): 577–590. doi:10.1016/j.devcel.2014.04.015.

LC3 Binding to the Scaffolding Protein JIP1 Regulates Processive Dynein-Driven Transport of Autophagosomes

Meng-meng Fu[1], **Jeffrey J. Nirschl**[1], and **Erika L. F. Holzbaur**[1,*]

[1]Department of Physiology, University of Pennsylvania Perelman School of Medicine, Philadelphia, PA 19104, USA

Abstract

Autophagy is essential for maintaining cellular homeostasis in neurons, where autophagosomes undergo robust unidirectional retrograde transport along axons. We find that the motor scaffolding protein JIP1 binds directly to the autophagosome adaptor LC3 via a conserved LIR motif. This interaction is required for the initial exit of autophagosomes from the distal axon, for sustained retrograde transport along the mid-axon, and for autophagosomal maturation in the proximal axon. JIP1 binds directly to the dynein activator dynactin, but also binds to and activates kinesin-1 in a phosphorylation-dependent manner. Following JIP1 depletion, phosphodeficient JIP1-S421A rescues retrograde transport, while phosphomimetic JIP1-S421D aberrantly activates anterograde transport. During normal autophagosome transport, residue S421 of JIP1 may be maintained in a dephosphorylated state by autophagosome-associated MKP1 phosphatase. Moreover, binding of LC3 to JIP1 competitively disrupts JIP1-mediated activation of kinesin. Thus, dual mechanisms prevent aberrant activation of kinesin to ensure robust retrograde transport of autophagosomes along the axon.

Keywords

JIP1; LC3; autophagy; axonal transport; kinesin; dynein; dynactin

Protein quality control and degradation play important roles in cellular homeostasis. In addition to the ubiquitin-proteasome pathway, cells utilize macroautophagy (henceforth referred to as autophagy) to selectively target misfolded or aggregated proteins and defective organelles for removal. Autophagy is essential in neurons as knockout of genes in this pathway leads to neuronal cell death (Hara et al., 2006; Komatsu et al., 2006). Defects in autophagy are associated with neurodegenerative diseases including Alzheimer's (Lee et al., 2011), Parkinson's (Ashrafi and Schwarz, 2013; Dagda et al., 2009; Lynch-Day et al., 2012; Narendra et al., 2008), Huntington's (Martinez-Vicente et al., 2010; Wong and Holzbaur, 2014) and amyotrophic lateral sclerosis (ALS) (Ravikumar et al., 2005; Rubino et al., 2012).

*Correspondence: holzbaur@mail.med.upenn.edu, Telephone: 1-215-573-3257, Fax: 1-215-573-5851.

The fidelity of the autophagic process may be particularly relevant in neurons for two reasons. First, accumulation of misfolded proteins and organelles may be especially toxic to neurons since they are post-mitotic. Second, neuronal processes may present a spatial challenge for efficient clearance of proteins and organelles via autophagy.

In the axon, autophagosomes undergo long-range microtubule-based retrograde transport that is coupled to compartment maturation (Hollenbeck, 1993; Lee et al., 2011; Maday et al., 2012). Thus, autophagosome transport dynamics along the axon are spatially regulated. In primary dorsal root ganglion (DRG) neurons, autophagosomes form preferentially in the distal axon tip and initially undergo inefficient back-and-forth bidirectional transport followed by a switch to unidirectional retrograde motility. In the mid-axon, autophagosomes rarely exhibit pauses or switches in direction (Maday et al., 2012). In cortical neurons, autophagosomes also exhibit unidirectional retrograde transport along the axon (Lee et al., 2011). The pronounced unidirectional transport characteristic of autophagosomes requires the microtubule motor dynein (Maday et al., 2012) and differs from the movement of other organelles in the axon, such as lysosomes (Moughamian and Holzbaur, 2012), amyloid precursor protein (APP) vesicles (Fu and Holzbaur, 2013; Stokin et al., 2005), mitochondria (Morris and Hollenbeck, 1993), and RNA granules (van Niekerk et al., 2007), which exhibit both anterograde and retrograde motility. Surprisingly, however, live-cell imaging and organelle isolation indicate that both dynein and the anterograde motor kinesin remain bound to axonal autophagosomes (Maday et al., 2012). Thus, retrograde axonal transport of autophagosomes must be tightly regulated in order to promote dynein motor activity while inhibiting the activity of associated kinesins.

A candidate coordinator of dynein and kinesin-1 activity is the motor scaffolding protein JIP1, known to regulate the highly processive transport of APP (Fu and Holzbaur, 2013; Muresan and Muresan, 2005). Direct binding of JIP1 to kinesin heavy chain (KHC), the motor subunit of kinesin-1, is sufficient to activate KHC motility. JIP1 also directly binds to the $p150^{Glued}$ subunit of the dynein activator dynactin. Importantly, JIP1 cannot simultaneously bind to both KHC and dynactin and instead forms either an anterograde or retrograde motor complex. In the retrograde complex, binding of dynactin to JIP1 disrupts the ability of JIP1 to activate KHC motility. Phosphorylation of JIP1 at S421 acts as a directional switch by increasing the affinity of JIP1 for KHC, favoring the formation of the anterograde complex and thus preferentially enhances anterograde over retrograde motility (Fu and Holzbaur, 2013).

Here, we demonstrate that JIP1 functions more broadly in axonal transport, also regulating the unidirectional retrograde transport of autophagosomes in a cargo-specific manner. JIP1 associates with autophagosomes via direct binding to the autophagosome adaptor LC3. While knockdown of JIP1 does not affect autophagosome biogenesis in the distal axon tip, JIP1 depletion inhibits the ability of autophagosomes to exit from the distal axon, to sustain retrograde transport along the mid-axon, and to mature normally in the proximal axon. Expression of phosphodeficient JIP1-S421A rescues retrograde autophagosome transport induced by JIP1 depletion, while expression of phosphomimetic JIP1-S421D leads to aberrant anterograde autophagosome transport, suggesting that sustained retrograde motility requires continued inhibition of KHC activation by JIP1. The phosphatase MKP1

colocalizes with JIP1 on autophagosomes and may function to prevent aberrant phosphorylation of JIP1. Furthermore, we find that direct binding of LC3 to JIP1 disrupts the ability of JIP1 to activate KHC motility *in vitro*. Thus, LC3 binding to JIP1 functions not only to mediate autophagosome association, but also as a cargo-specific mechanism to regulate motor coordination and to sustain efficient retrograde motility. These experiments establish JIP1 as a versatile scaffolding protein capable of regulating the transport of diverse cargos along the axon.

EXPERIMENTAL PROCEDURES

Cell Culture and Transfection

DRGs dissected from adult wildtype or transgenic GFP-LC3 mice (Mizushima, 2004) less than 1 year old were dissociated (Perlson et al., 2009), electroporated and plated on glass coverslips or glass-bottom microwell dishes coated with poly-L-lysine and laminin (see Supplemental Experimental Procedures for details).

For Rab7 motility assays, wildtype DRGs were co-transfected with EGFP-Rab7 and fluorescent DY-547-conjugated JIP1 siRNA (5'-GAGCAAACCCAUCGGGCUAUU-3'; Dharmacon). For Rab7/LC3 co-migration studies, wildtype DRGs were co-transfected with EGFP-Rab7 and mCherry-LC3. For distal axon co-migration assays, wildtype DRGs were transfected with EGFP-JIP1 and mCherry-LC3. For JIP1 knockdown and rescue experiments, neurons from GFP-LC3 mice were transfected with DY-547-conjugated JIP1 siRNA and a bidirectional construct co-expressing the fluorescent marker BFP and wildtype or mutant JIP1 [pBI-CMV2(BFP)-JIP1(WT, S421A, S421D, or ΔLIR)]. To examine autophagosome acidification, wildtype DRGs were transfected with mCherry-GFP-LC3, non-fluorescent JIP1 siRNA and pBI-CMV2(BFP)-JIP1-ΔLIR.

Live-cell Microscopy

Cultured DRGs were imaged at 2 DIV in Hibernate A low-fluorescence medium (Brain Bits) inside a 37°C chamber. For transport assays, neurons were observed at 63x using a DMI6000B epifluorescence microscope with a CTR7000 HS control box run by LAS-AF6000 software (Leica) and a C10600 Orca-R2 camera (Hamamatsu); images were acquired at 3 seconds per frame for 3 minutes. For axon tip biogenesis and distal axon exit assays, GFP-LC3 neurons were observed at 100x with the 488-nm and 562-nm laser on an Ultraview Vox spinning-disk confocal system (PerkinElmer) on an inverted Ti microscope (Nikon); images were acquired at 1–2 seconds per frame for 5–10 minutes. Frame rates were optimized for each experimental approach (epifluorescence versus confocal) to capture events with high time resolution while minimizing photobleaching; within an experiment all conditions were imaged with the same paradigm.

Vesicle Tracking and Analysis

Four distinct axonal regions were analyzed: 1) the axon tip, the most distal region of the axon that is usually fan-shaped; 2) the distal axon, the region immediately proximal to the axon tip; 3) the mid-axon, a region >100 μm from both the soma and the axon tip; and 4) the proximal axon, a region <100 μm from the soma (Figure 4A). The boundary between the

axon tip and the distal axon was defined as the region where the axon tip narrows to twice the width of the axon (defined at 50 μm away from the end of the axon tip), usually a width of ~1–2 μm.

Motility of Rab7-positive and LC3-positive vesicles was analyzed by generating 75-μm kymographs using Metamorph software. Motile vesicles (e.g. anterograde or retrograde) were defined by net displacement >10 μm while bidirectional/stationary vesicles were defined by net displacement <10 μm. Speed and run length values were calculated from the net velocity and net displacement of individual vesicles. Switches were defined as changes in direction preceded and succeeded by runs >1 μm. The neuron was defined as the biologically relevant unit and motility parameters were averaged for each neuron.

Immunofluorescence Staining

Cultured DRGs were stained with antibodies to JIP1 (mouse monoclonal Santa Cruz B-7 or sheep polyclonal R&D Systems), LC3 (mouse monoclonal MBL Japan), MKP7 (rabbit polyclonal Genetex C2C3), and MKP1 (rabbit polyclonal Santa Cruz V-15); see Supplemental Experimental Procedures for details. For quantification of colocalization, 20-μm kymographs were generated in the mid-axon and puncta with intensity greater than the half-max value was defined as positive for either LC3 or JIP1.

Organelle Purification

Autophagosome-enriched fractions were prepared from wildtype adult mouse brains following a three-step protocol (Maday et al., 2012; Stromhaug et al., 1998) and subject to BCA assays to ensure equal loading. Western blots were probed with antibodies to LC3 (Abcam), JIP1 (B-7 Santa Cruz), $p150^{Glued}$ (BD Transduction), and DIC (Chemicon).

Co-immunoprecipitations

Immunoprecipitations were performed from mouse brain homogenates or transfected COS7 cell lysates using Protein-G Dynabeads (Invitrogen) and monoclonal antibodies against JIP1 (Santa Cruz B-7), LC3 (MBL Japan), or myc (Invitrogen); see Supplemental Experimental Procedures for details. Densitometry quantification was performed using the Gel Analyzer function of ImageJ. All co-immunoprecipitations represent at least two independent experiments.

Recombinant Protein Binding Assay

For binding assays, recombinant untagged JIP1 was incubated 30 minutes at room temperature with glutathione beads bound to either purified GST or GST-LC3 (Enzo Life Sciences), washed, and eluted with glutathione; see Supplemental Experimental Procedures for details.

In vitro COS7 Lysate Motility Assay

COS7 cells transfected with KHC-head-Halo (KIF5C[1–560]) or KHC-Halo were incubated with TMR ligand (Promega) and lysed. Cell lysates were introduced into flow chambers with taxol-stabilized microtubules bound to the coverslip; see Supplemental Experimental Procedures for details.

For each set of experiments, we conducted at least 3 independent trials, each with fresh lysate. To minimize variation, each chamber contained equal amounts of microtubules, KHC-Halo lysate, and total lysate (by adding nontransfected lysate). Multiple videos were acquired for each condition at 3 frames per second for 1 minute at room temperature using an Ultraview Vox TIRF system (PerkinElmer) on an inverted Ti microscope (Nikon) with the 100x objective and an ImagEM C9100-13 camera (Hamamatsu Photonics) controlled by Volocity software. Kymographs of microtubules with lengths >10 μm were analyzed for run frequency, which were normalized with respect to microtubule length. Individual runs were measured at the level of each motile particle (i.e. each particle has one run length or net displacement and one speed measurement).

Statistical analysis

Statistical analysis was performed using Student's t-test for experiments with 2 conditions and one-way ANOVA with post-hoc Dunnett's Test (comparing against the no knockdown control condition) for experiments with >2 conditions. Bar graphs show mean ± SEM with the following denotations for statistical significance: * $p<0.05$, ** $p<0.01$, *** $p<0.001$, n.s. (not significant).

RESULTS

JIP1 Knockdown Disrupts Transport of Rab7-Positive Vesicles

JIP1 regulates the transport of diverse classes of vesicular cargo, including synaptic vesicles and mitochondria in *Drosophila* neurons (Horiuchi et al., 2005) and APP-positive vesicles in mammalian neurons (Fu and Holzbaur, 2013; Muresan and Muresan, 2005). Immunostaining of primary DRG neurons shows co-localization of JIP1 with APP along the axon, but also suggests that JIP1 may localize to other organelle compartments (Fu and Holzbaur, 2013).

To determine whether JIP1 mediates the axonal transport of additional organelles in mammalian neurons, we asked if the transport of Rab7-positive late endosomes (Deinhardt et al., 2006) is dependent on JIP1. We knocked down endogenous mouse JIP1 in primary DRG neurons using a targeted siRNA that depletes >90% of JIP1 without detectable off-target effects (Fu and Holzbaur, 2013). Following electroporation of red fluorescent JIP1 siRNA and an EGFP-Rab7 construct, we imaged transport in the mid-axon and quantitated motility by generating kymographs (Figure 1A). In control neurons, the majority of Rab7-positive vesicles exhibit bidirectional or stationary motility defined by net displacement <10 μm (72.5 ± 2.3%). Motile Rab7-positive vesicles, defined by net displacement >10 μm over our imaging period, moved predominantly in the retrograde direction (26.6 ± 2.4%) and rarely in the anterograde direction (0.9 ± 0.7%; Figure 1B).

JIP1 knockdown did not affect the density of Rab7-positive vesicles along the axon (control: 0.33 ± 0.02 vesicles per μm; JIP1 knockdown: 0.36 ± 0.02 vesicles per μm; $p = 0.30$), but did alter their motility. JIP1 depletion decreased the percentage of retrograde-moving vesicles by 68% ($p<0.001$) and commensurately increased the percentage of bidirectional/stationary vesicles ($p<0.001$, Figure 1B). The subpopulation of Rab7-positive vesicles that

continue to move in the retrograde direction in JIP1-depleted neurons displayed unaltered motility with no significant changes in net displacement (control: 22.4 ± 1.3 μm/s; JIP1 knockdown: 23.2 ± 2.4 μm/s; p = 0.79) or net speed (control: 0.43 ± 0.03 μm/s; JIP1 knockdown: 0.50 ± 0.07 μm/s; p = 0.37). Thus, there are two subpopulations of Rab7-positive vesicles moving along axons; while the movement of one subpopulation is independent of JIP1, we find that JIP1 depletion arrests a distinct sub-population of retrograde Rab7-positive organelles.

Classic experiments in chick DRG axons showed that retrograde phase-dense vesicles are both endosomal and autophagosomal in nature (Hollenbeck, 1993). In axons of DRGs and cortical neurons, autophagosomes co-migrate with LAMP1, a marker for late endosomes (Lee et al., 2011; Maday et al., 2012), suggesting that autophagosomes fuse with endosomes to form amphisomes in the axon. Moreover, the speed and displacement of the JIP1-dependent retrograde Rab7-positive vesicles resemble the characteristic unidirectional retrograde motility of autophagosomes (Maday et al., 2012). Thus, we hypothesized that this subpopulation of retrograde Rab7-positive vesicles affected by JIP1 knockdown are autophagosomes. To verify this, we co-transfected DRGs with EGFP-Rab7 and the autophagosome marker mCherry-LC3 (Figure 1C, 1E and Movie S1). The majority of retrograde Rab7-positive vesicles with net displacement >10 μm co-migrate with mCherry-LC3 (64.7 ± 7.5%) in the mid-axon. In contrast, few bidirectional/stationary Rab7-positive vesicles are positive for mCherry-LC3 (22.6 ± 8.6%, Figure 1D). Of note, the percentage of retrograde Rab7-positive vesicles that are LC3-positive (65%) is similar to the 68% decrease in retrograde Rab7-positive vesicles observed following JIP1 knockdown (Figure 1B), suggesting that LC3-positive organelles are preferentially susceptible to JIP1 depletion.

JIP1 Associates with Autophagosomes

To follow up on this observation, we examined the possible association of JIP1 with autophagosomes. First, we purified autophagosomes from wildtype mouse brain by differential centrifugation (Maday et al., 2012; Stromhaug et al., 1998). Whereas cytosolic LC3-I (~18 kD) is enriched in brain homogenate, membrane-bound lipidated LC3-II (~16 kD) is enriched in the autophagosome fraction (Kabeya et al., 2000). A comparison of the initial brain homogenate and cytosolic fractions indicates that JIP1 is also enriched in the autophagosome fraction (Figure 2A). Interestingly, high-molecular-weight JIP1 (~110 kD) was enriched in the autophagosome fraction while low-molecular-weight JIP1 (~90 kD) was not, suggesting that differentially spliced JIP1 isoforms may preferentially associate with different organelles. To further explore this association, we used an anti-LC3 antibody to immunoprecipitate LC3 from mouse brain homogenate and found that endogenous JIP1 coimmunoprecipitated with this fraction (Figure 2B), suggesting that endogenous LC3 and JIP1 form a complex.

Next, we stained non-transfected wildtype DRG neurons for JIP1 and LC3 and observed that large JIP1-positive puncta colocalized with LC3 along the axon (Figure 2C). Quantification shows that 72 ± 2% (n = 10 neurons) of LC3-positive puncta were also JIP1-positive. We also noted some colocalization of JIP1 and LC3 at axon tips, although to a lesser extent than was observed along the axon (Figure 2D).

JIP1 Binds to the Autophagosome Adaptor LC3

One mechanism for motor adaptor association with autophagosomes is via direct binding to LC3; the adaptors FYCO1 and optineurin, which have been proposed to regulate kinesin and myosin activity, respectively, both bind to LC3 via a conserved LIR (LC3-interacting region) motif (Pankiv et al., 2010; Wild et al., 2011). To test for an association between JIP1 and LC3, we immunoprecipitated lysates from COS7 cells co-transfected with GFP-LC3 and myc-JIP1. Indeed, an anti-myc antibody coimmunoprecipitated full-length myc-JIP1 as well as GFP-LC3 (Figure 3A).

Next, we used purified recombinant proteins to confirm that JIP1 binds directly to LC3. GST-JIP1 expressed in *E. coli* was purified and subsequently cleaved to generate untagged JIP1. JIP1 was loaded onto glutathione columns with either GST or GST-LC3 bound to the matrix; bound proteins were then eluted with glutathione. In the control condition, JIP1 did not bind to GST and the majority of JIP1 was found in the flow-through fraction. In contrast, JIP1 bound robustly to GST-LC3 with no detectable JIP1 remaining in the flow-through (Figure 3B).

To further map the binding site for LC3 on JIP1, we performed coimmunoprecipitations from lysates of COS7 cells co-transfected with GFP-LC3 and truncated myc-JIP1 constructs. C-terminal myc-JIP1[445-565] and myc-JIP1[554-711] did not coimmunoprecipitate GFP-LC3. However, N-terminal myc-JIP1[307-711] robustly coimmunoprecipitated GFP-LC3, as did myc-JIP1[1-390], though to a lesser extent (Figure 3A). Thus, the region spanning AA307-390, where these two constructs overlap, may be a putative LC3-binding domain.

This region of JIP1 contains a predicted LIR motif, EEEEGFDCL (Figure 3C). LIRs contain the core consensus sequence [W/F/Y]xx[L/I/V] and acidic residues frequently flank the aromatic residue (Birgisdottir et al., 2013). The intermolecular interactions underlying LIR binding to LC3 are well characterized. The LIR of the autophagosome cargo adaptor p62 (DDDWTHL) binds inside a narrow groove in LC3 (Figure 3D), with the aromatic residue and the leucine binding to hydrophobic pockets in LC3 and the three consecutive aspartic acids interacting with basic residues in the N-terminus of LC3 (Ichimura et al., 2008; Noda et al., 2008). Similar to FYCO1 and optineurin, JIP1 contains a F-type LIR with a phenylalanine residue at the aromatic position. Multiple sequence alignments of F-type LIRs (Figure 3E) show that these conserved residues are conserved in mammalian JIP1 LIRs (Figure 3C).

We generated JIP1 mutants lacking the LIR (ΔLIR) or containing a mutation in the phenylalanine residue (F336A). In coimmunoprecipitations from COS7 cells co-transfected with myc-JIP1 and GFP-LC3 constructs, myc-JIP1-ΔLIR and F336A exhibited significantly decreased binding to GFP-LC3 as compared to wildtype myc-JIP1 (Figure 3F). Thus, the LIR motif we identified in JIP1 is necessary for robust binding to LC3. Because both JIP1 LIR mutants contain intact SH3 homodimerization domains (Kristensen et al., 2006), their residual binding to LC3 may be attributed to dimerization with endogenous wildtype JIP1.

The observation that JIP1 directly binds to LC3 via its LIR motif, together with immunostaining, coimmunoprecipitation, and co-fractionation results, establishes JIP1 as an autophagosome adaptor. In order to elucidate the function of JIP1, we asked how JIP1 may affect autophagosome biology in 4 distinct axonal regions – the distal axon tip, the distal axon, the mid-axon, and the proximal axon.

Biogenesis of Autophagosomes in the Axon Tip Does Not Require JIP1

In the CAD neuronal cell line and in DRGs, JIP1 accumulates in distal neurite or axon tips (Fu and Holzbaur, 2013; Muresan and Muresan, 2005; Verhey et al., 2001). Moreover, a limited number of JIP1-positive puncta colocalize with LC3 at the distal axonal tip (Figure 2D). Since biogenesis of axonal autophagosomes in primary DRGs occurs exclusively in distal axonal tips (Maday et al., 2012), we asked whether JIP1 is necessary for autophagosome formation. Using time-lapse live-cell confocal microscopy of primary DRGs cultured from GFP-LC3 mice (Mizushima, 2004), we observed continuous autophagosome biogenesis in the distal axon tip (Figure 4A). Initially, small punctate LC3-positive structures become visible and then gradually enlarge to form a ring-like structure up to ~1 μm in diameter. These events occur on the timescale of several minutes (Figure 4B and Movie S2), consistent with previously published observations (Maday et al., 2012).

JIP1 depletion did not significantly decrease the density of autophagosomes in the axon tip (control: 0.135 ± 0.018 autophagosomes per μm^2; JIP1 knockdown: 0.162 ± 0.013 autophagosomes per μm^2; $p = 0.24$; Figure 4C, 4D), further confirming that biogenesis of this organelle does not depend on JIP1. Further, the lack of accumulation of autophagosomes in JIP1-depleted axon tips suggests that JIP1 is not required for the exit of autophagosomes from the axon tip into the distal axon, which we define as a distinct region immediately proximal to the axon tip.

Efficient Exit of Autophagosomes from the Distal Axon Requires JIP1

In primary DRGs, most autophagosomes in the distal axon exhibit bidirectional/stationary motility, while autophagosomes in the mid-axon exhibit robust retrograde motility (Maday et al., 2012). Thus, we hypothesized that maturing autophagosomes undergo a switch from bidirectional/stationary motility to retrograde motility upon recruitment of JIP1. To test this idea, we performed co-migration assays in the distal axon (Figure 4A) of DRGs co-transfected with EGFP-JIP1 and mCherry-LC3 (Figure 4E and Movie S3). Autophagosomes were classified as either EGFP-JIP1-positive or EGFP-JIP1-negative and also categorized as motile or bidirectional/stationary. EGFP-JIP1-positive autophagosomes exhibited 3-times the retrograde motility of EGFP-JIP1-negative autophagosomes (Figure 4F), indicating that JIP1-associated autophagosomes are more likely to transit from the distal axon into the mid-axon.

If JIP1 recruitment to autophagosomes is important for initiating retrograde motility in the distal axon, then JIP1 depletion should lead to organelle accumulation in this region. Indeed, JIP1 knockdown results in autophagosome accumulation in the distal axon, most strikingly in the region closest to the axon tip (Figures 4G and 4H). This accumulation likely results from inefficient initiation of retrograde transport of autophagosomes from the distal axon

and therefore is consistent with the decreased percentage of retrograde autophagosome motility observed in the distal axons of JIP1-depleted neurons (Figure 4I).

Processive Retrograde Autophagosome Transport in the Mid-Axon Requires Nonphosphorylated JIP1

Next, we asked whether JIP1 is necessary to sustain robust retrograde autophagosome transport along the mid-axon (Figure 4A). We found that JIP1 knockdown significantly decreased the percentage of retrograde autophagosomes from ~70% to ~40%, concurrent with a significant increase in the percentage of bidirectional/stationary autophagosomes, from ~30% to ~60% (Figures 5A, 5B and Movie S4). Autophagosomes that continued to move in the retrograde direction in JIP1-depleted neurons displayed significantly lower net displacement and net speed than autophagosome from control neurons (Figures 5C and 5D), consistent with a trend toward more directional switches (Figure 5E). Thus, in the absence of JIP1, even autophagosomes that continue to move in the retrograde direction displayed impaired motility.

The characteristic retrograde motility of autophagosomes in the mid-axon depends on dynein activity, but paradoxically, purified autophagosomes maintain a tight association with kinesins (Maday et al., 2012). Together, these observations suggest that autophagosome-associated kinesins are autoinhibited. As a scaffolding protein that binds directly to both kinesin and to dynactin, JIP1 can coordinate opposing motor activity. Endogenous JIP1 in the brain is phosphorylated as treatment with phosphatase leads to decreased molecular weight (Fu and Holzbaur, 2013). While site-directed mutagenesis and mass spectrometry identified more than 35 phosphorylation sites in JIP1 (D'Ambrosio et al., 2006; Nihalani et al., 2003), we found that phosphorylation of S421, located within the KHC-tail-binding domain, regulates the binding affinity of JIP1 for KHC. Phosphorylation of S421 switches JIP1 from a dynactin-bound conformation to a KHC-bound conformation. Phosphomimetic JIP1-S421D has increased affinity for KHC tail, leading to preferential enhancement of anterograde APP axonal transport while phosphodeficient JIP1-S421A binds to KHC tail with much lower affinity, leading to the preferential enhancement of retrograde APP axonal transport (Fu and Holzbaur, 2013).

We asked whether JIP1 phosphorylation also regulates autophagosome motility by performing knockdown and rescue experiments with siRNA-resistant human JIP1 phosphomutants. Expression of JIP1-S421A robustly restored the percentage of retrograde autophagosomes as well as net displacement and speed (Figures 5B–5D). In contrast, JIP1-S421D expression decreased the percentage of retrograde autophagosomes to ~20% and increased the percentage of bidirectional/stationary autophagosomes to ~70% along the mid-axon (Figure 5B). Retrograde autophagosomes in JIP1-S421D-expressing neurons move with reduced net displacement (Figure 5C), consistent with a trend toward higher incidences of directional switches (Figure 5E). In the mid-axon of control neurons, typically <1% of autophagosomes move in the anterograde direction, but neurons expressing JIP1-S421D display an unusually high percentage (~10%) of anterograde autophagosomes (Figure 5B). Thus, expression of JIP1-S421D disrupts normal retrograde autophagosome transport and

aberrantly activates anterograde autophagosome transport, likely due to enhanced binding to KHC.

These results suggest that sustained retrograde autophagosome transport requires nonphosphorylated JIP1 that cannot efficiently bind and activate KHC. JIP1 is a scaffolding protein known to bind to both kinases and phosphatases, so we asked whether a JIP-associated phosphatase might act to sustain retrograde transport by maintaining S421 in a nonphosphorylated state. We screened two MAPK phosphatases – MKP7, which directly binds to JIP1 (Willoughby et al., 2003) and MKP1, an axon-specific phosphatase that affects axon outgrowth (Jeanneteau et al., 2010). Immunostaining of nontransfected DRGs shows that MKP7 and JIP1 do not colocalize in the axon (Figure S1A) while MKP1 and JIP1 robustly colocalize using two different JIP1 antibodies (Figure S1B, Figure 5F). Though we do not yet know whether JIP1 and MKP1 bind directly, they do colocalize on LC3-positive puncta (Figure 5F), indicating that this phosphatase is strategically localized to maintain nonphosphorylated S421 during the retrograde transit of autophagosomes along the axon.

LC3 Binding Inhibits JIP1-Mediated Activation of Kinesin *in vitro*

In the primary structure of JIP1, the LIR motif (~AA340) is located near the KHC-tail-binding domain (AA390–440 (Fu and Holzbaur, 2013); Figure 3C). The proximity of these binding domains led us to hypothesize that LC3 binding may sterically hinder KHC tail from binding to JIP1 and consequently inhibit JIP1-dependent activation of KHC motility. To address this idea functionally, we performed *in vitro* single-molecule motility assays using lysates of COS7 cells transfected with full-length KHC (Blasius et al., 2007; Sun et al., 2011). When applied to flow chambers containing immobilized blue microtubules, red fluorescent KHC-Halo from COS7 lysates can be visualized by total internal reflection fluorescence (TIRF) microscopy (Figures 6A, 6B and Movie S5). Consistent with our previous observations, autoinhibited KHC-Halo exhibits few processive runs, but addition of myc-JIP1 lysate significantly increased run frequency, run length and speed of KHC-Halo (Figures 6B–6F).

Next, we asked how addition of GFP-LC3 lysate would affect JIP1-mediated KHC activation. LC3 was originally identified as a microtubule-associated protein (Mann and Hammarback, 1994); indeed, GFP-LC3 decorates microtubules in our flow chambers, but binding of LC3 to microtubules does not inhibit the motility of Halo-tagged constitutively active KHC head (KHC head: 0.35 ± 0.05 μm/s; KHC head +GFP-LC3: 0.27 ± 0.01 μm/s; p=0.16; n = 94–230 runs). In contrast, addition of GFP-LC3 in the presence of myc-JIP1 significantly decreased the speed, run frequency, and run length of KHC-Halo (Figures 6D–6F). Thus, addition of LC3 perturbs the ability of JIP1 to activate KHC motility *in vitro*.

LIR Motif is Required for Efficient Retrograde Autophagosome Transport

The LIR motif of JIP1 likely plays dual roles – both inducing JIP1 recruitment to the autophagosome and preventing kinesin activation by autophagosome-associated JIP1. To confirm the importance of the JIP1 LIR motif for autophagosome transport in neurons, we performed knockdown and rescue experiments in DRGs with the JIP1-ΔLIR and F336A mutants, which have decreased binding to LC3 (Figure 3F) and likely cannot be recruited to

autophagosomes. Indeed, motility of autophagosomes in the mid-axon of neurons rescued with JIP1-ΔLIR or F336A is similar to that of JIP1-depleted neurons, with most autophagosomes exhibiting either bidirectional/stationary movement (~55–60%; Figures 6G, 6H and Movie S4). Neurons expressing JIP1-ΔLIR or F336A exhibit a low percentage of retrograde autophagosomes (~30–40%), which display decreased net displacement, and a relatively high percentage of aberrantly anterograde autophagosomes (~5–10%; Figures 6H–6J). Thus, JIP1 LIR mutants are insufficient to rescue retrograde autophagosome transport in the mid-axon.

JIP1 Binding to LC3 is Necessary for Autophagosome Acidification in the Proximal Axon

Next we asked whether impaired autophagosome transport induced by expression of mutant JIP1 might lead to impaired autophagosome function. Degradation of engulfed cargos requires autophagosome fusion with lysosomes. Lysosomal fusion results in increased acidification of autophagosomes, which can be monitored with the dual-color reporter mCherry-GFP-LC3. Prior to fusion with lysosomes, autophagosomes expressing this construct appear yellow; upon lysosomal fusion and acidification, preferential quenching of the GFP moiety results in a shift to red-only autophagosomes (Pankiv et al., 2010). We transfected this construct into wildtype DRGs and measured the fraction of mature versus immature autophagosomes (Figures 7A–7D). In wildtype neurons, the percentage of immature mCherry- and GFP-positive autophagosomes is ~50% in the distal axon and ~30% in the proximal axon (Figure 7D), consistent with a model in which autophagosomes fuse with lysosomes as they undergo retrograde transport along the axon (Maday et al., 2012). Upon knockdown of endogenous JIP1 and expression of the JIP1-ΔLIR mutant, the percentage of immature mCherry- and GFP-positive autophagosomes in the proximal axon increased to ~50%, similar to the level in wildtype distal axons (Figure 7D). Thus, expression of a JIP1 construct that cannot bind LC3 both impairs retrograde autophagosome transport and induces a parallel defect in compartment acidification.

DISCUSSION

Here, we show that the scaffolding protein JIP1 regulates transport in a cargo-dependent manner. Further, we show that multiple mechanisms ensure that autophagosomes move processively in the retrograde direction along the axon. JIP1 knockdown inhibits the exit of autophagosomes from the distal axon, results in failure to sustain robust retrograde autophagosome transport in the mid-axon, and hinders acidification of autophagosomes reaching the proximal axon. Moreover, knockdown and rescue with phosphomimetic JIP1-S421D, which robustly binds to KHC tail, does not rescue retrograde autophagosome motility in the mid-axon and instead results in aberrant anterograde transport of autophagosomes. Thus, one mechanism for sustaining retrograde autophagosome transport in the axon requires the maintenance of S421 of JIP1 in a nonphosphorylated state that cannot efficiently activate KHC. The strategic localization of the phosphatase MKP1 to JIP1-positive autophagosomes likely maintains this state. In a second and complementary mechanism, direct binding of JIP1 to LC3 via a LIR motif perturbs the ability of JIP1 to activate KHC motility *in vitro*, thus serving as an additional cargo-specific mechanism to maintain retrograde transport.

Together, these data support a model whereby autophagosomes in the distal axon initially bind to both kinesin and dynein motors, whose opposing and unregulated activity produces a tug-of-war leading to bidirectional motility with frequent directional switching. Subsequently, JIP1 is recruited to autophagosomes via direct binding to LC3, an interaction that blocks the binding of JIP1 to KHC and thus prevents aberrant KHC activation. JIP1-positive autophagosomes then switch to highly processive retrograde motility, moving efficiently from the distal axon toward the cell soma. The effective inhibition of kinesin motility results in sustained retrograde transport along the mid-axon (Figure 7E). The dynactin-bound retrograde JIP1 complex cannot bind to KHC, but can simultaneously associate with kinesin light chain (KLC), the adaptor subunit of kinesin-1 (Fu and Holzbaur, 2013) via an independent binding site in the C-terminus of JIP1 (Verhey et al., 2001), which may serve as a mechanism for the retention of autoinhibited kinesin on the autophagosome.

To date, JIP1 is the only identified scaffolding protein that directly links dynactin to autophagosomes in an LC3-dependent manner. However, multiple scaffolding proteins may cooperate for efficient retrograde transport in the axon, as biochemical quantification of endosomes or lysosomes purified from brain (Hendricks et al., 2010) and optical trapping of phagosomes in rodent macrophage cell lines indicate that robust retrograde transport correlates with 6–12 cargo-associated dynein molecules (Hendricks et al., 2012; Rai et al., 2013). Indeed, neurons deficient for the small adaptor protein Snapin, which binds to DIC, also show dramatic disruption of Rab7-positive vesicle transport in the axon and defects in autophagosome clearance (Cai et al., 2010). The large scaffolding protein huntingtin, which also binds to DIC (Caviston et al., 2007) and mediates transport of endosomes (Caviston et al., 2011), also mediates autophagosome transport along the axon, potentially of a distinct subpopulation (Wong and Holzbaur, 2014). Finally, the Rab7 effector RILP (Rab7-interacting lysosomal protein), which recruits dynactin to late endosomes in non-neuronal cells (Johansson et al., 2007), has been implicated in autophagosome clearance in Purkinje neurons (Bains et al., 2011). As autophagosomes display increased overall retrograde motility (~70%) compared to Rab7-positive vesicles (~25%), autophagosomes may have enhanced ability to recruit or to retain dynein, perhaps via fusion with endosomes, resulting in associations with multiple scaffolding proteins.

Knockdown of JIP1 does not impair the total number of autophagosomes in the axon tip (Figure 4D), indicating that the both biogenesis and initial exit from the axon tip does not require JIP1. The motility of newly formed autophagosomes in the distal axon tip may be driven by kinesin and myosin via their respective motor adaptors, FYCO1 and optineurin (Pankiv et al., 2010; Tumbarello et al., 2012). Interestingly, FYCO1, which has been suggested to regulate kinesin activity, and the myosin adaptor optineurin both bind to LC3 via F-type LIRs (Pankiv et al., 2010; Wild et al., 2011). Mutagenic analysis indicates that F-type LIRs may not bind LC3 as robustly as W-based LIRs. However, serines often precede F-type LIRs (Birgisdottir et al., 2013) and phosphorylation at these sites may enhance the association between acidic residues in the LIR and basic residues in LC3, as demonstrated for optineurin (Rogov et al., 2013). Indeed, the serines preceding the JIP1 LIR are phosphorylated in mass spectrometry studies (D'Ambrosio et al., 2006) though they are not sites of direct phosphorylation by JNK (Nihalani et al., 2003). In contrast to W-type LIRs that function in initial cargo sequestration to autophagosomes, F-type LIRs found in motor

adaptors may be targeted for post-translational modification in order to navigate complex cellular environments and to respond to spatially specific signals.

Direct binding of JIP1 to LC3 provides a novel mechanism for regulation of transport by cargo association. Together, our observations firmly establish JIP1 as a versatile motor adaptor protein that regulates the retrograde axonal transport of autophagosomes and highlight the importance of motor coordination and cargo association in sustaining directed transport in the axon.

Supplementary Material

Refer to Web version on PubMed Central for supplementary material.

Acknowledgments

We gratefully acknowledge technical assistance from Mariko Tokito and Karen Wallace Jahn, insightful discussions with Sandra Maday, and funding to MMF (T32GM7517 and F31NS73262), JJN (T32GM7170), and ELFH (GM48661).

References

Ashrafi G, Schwarz TL. The pathways of mitophagy for quality control and clearance of mitochondria. Cell death and differentiation. 2013; 20:31–42. [PubMed: 22743996]

Bains M, Zaegel V, Mize-Berge J, Heidenreich KA. IGF-I stimulates Rab7-RILP interaction during neuronal autophagy. Neurosci Lett. 2011; 488:112–117. [PubMed: 20849920]

Birgisdottir AB, Lamark T, Johansen T. The LIR motif - crucial for selective autophagy. J Cell Sci. 2013; 126:3237–3247. [PubMed: 23908376]

Blasius TL, Cai D, Jih GT, Toret CP, Verhey KJ. Two binding partners cooperate to activate the molecular motor Kinesin-1. J Cell Biol. 2007; 176:11–17. [PubMed: 17200414]

Cai Q, Lu L, Tian JH, Zhu YB, Qiao H, Sheng ZH. Snapin-regulated late endosomal transport is critical for efficient autophagy-lysosomal function in neurons. Neuron. 2010; 68:73–86. [PubMed: 20920792]

Caviston JP, Ross JL, Antony SM, Tokito M, Holzbaur EL. Huntingtin facilitates dynein/dynactin-mediated vesicle transport. Proc Natl Acad Sci U S A. 2007; 104:10045–10050. [PubMed: 17548833]

Caviston JP, Zajac AL, Tokito M, Holzbaur EL. Huntingtin coordinates the dynein-mediated dynamic positioning of endosomes and lysosomes. Mol Biol Cell. 2011; 22:478–492. [PubMed: 21169558]

D'Ambrosio C, Arena S, Fulcoli G, Scheinfeld MH, Zhou D, D'Adamio L, Scaloni A. Hyperphosphorylation of JNK-interacting protein 1, a protein associated with Alzheimer disease. Mol Cell Proteomics. 2006; 5:97–113. [PubMed: 16195223]

Dagda RK, Cherra SJ 3rd, Kulich SM, Tandon A, Park D, Chu CT. Loss of PINK1 function promotes mitophagy through effects on oxidative stress and mitochondrial fission. J Biol Chem. 2009; 284:13843–13855. [PubMed: 19279012]

Deinhardt K, Salinas S, Verastegui C, Watson R, Worth D, Hanrahan S, Bucci C, Schiavo G. Rab5 and Rab7 control endocytic sorting along the axonal retrograde transport pathway. Neuron. 2006; 52:293–305. [PubMed: 17046692]

Fu MM, Holzbaur EL. JIP1 regulates the directionality of APP axonal transport by coordinating kinesin and dynein motors. J Cell Biol. 2013

Hara T, Nakamura K, Matsui M, Yamamoto A, Nakahara Y, Suzuki-Migishima R, Yokoyama M, Mishima K, Saito I, Okano H, et al. Suppression of basal autophagy in neural cells causes neurodegenerative disease in mice. Nature. 2006; 441:885–889. [PubMed: 16625204]

Hendricks AG, Holzbaur EL, Goldman YE. Force measurements on cargoes in living cells reveal collective dynamics of microtubule motors. Proc Natl Acad Sci U S A. 2012; 109:18447–18452. [PubMed: 23091040]

Hendricks AG, Perlson E, Ross JL, Schroeder HW 3rd, Tokito M, Holzbaur EL. Motor Coordination via a Tug-of-War Mechanism Drives Bidirectional Vesicle Transport. Curr Biol. 2010; 20:697–702. [PubMed: 20399099]

Hollenbeck PJ. Products of endocytosis and autophagy are retrieved from axons by regulated retrograde organelle transport. J Cell Biol. 1993; 121:305–315. [PubMed: 7682217]

Horiuchi D, Barkus RV, Pilling AD, Gassman A, Saxton WM. APLIP1, a kinesin binding JIP-1/JNK scaffold protein, influences the axonal transport of both vesicles and mitochondria in Drosophila. Curr Biol. 2005; 15:2137–2141. [PubMed: 16332540]

Ichimura Y, Kumanomidou T, Sou YS, Mizushima T, Ezaki J, Ueno T, Kominami E, Yamane T, Tanaka K, Komatsu M. Structural basis for sorting mechanism of p62 in selective autophagy. J Biol Chem. 2008; 283:22847–22857. [PubMed: 18524774]

Jeanneteau F, Deinhardt K, Miyoshi G, Bennett AM, Chao MV. The MAP kinase phosphatase MKP-1 regulates BDNF-induced axon branching. Nat Neurosci. 2010; 13:1373–1379. [PubMed: 20935641]

Johansson M, Rocha N, Zwart W, Jordens I, Janssen L, Kuijl C, Olkkonen VM, Neefjes J. Activation of endosomal dynein motors by stepwise assembly of Rab7-RILP-p150Glued, ORP1L, and the receptor betalll spectrin. J Cell Biol. 2007; 176:459–471. [PubMed: 17283181]

Kabeya Y, Mizushima N, Ueno T, Yamamoto A, Kirisako T, Noda T, Kominami E, Ohsumi Y, Yoshimori T. LC3, a mammalian homologue of yeast Apg8p, is localized in autophagosome membranes after processing. EMBO J. 2000; 19:5720–5728. [PubMed: 11060023]

Komatsu M, Waguri S, Chiba T, Murata S, Iwata J, Tanida I, Ueno T, Koike M, Uchiyama Y, Kominami E, et al. Loss of autophagy in the central nervous system causes neurodegeneration in mice. Nature. 2006; 441:880–884. [PubMed: 16625205]

Kristensen O, Guenat S, Dar I, Allaman-Pillet N, Abderrahmani A, Ferdaoussi M, Roduit R, Maurer F, Beckmann JS, Kastrup JS, et al. A unique set of SH3-SH3 interactions controls IB1 homodimerization. EMBO J. 2006; 25:785–797. [PubMed: 16456539]

Lee S, Sato Y, Nixon RA. Lysosomal proteolysis inhibition selectively disrupts axonal transport of degradative organelles and causes an Alzheimer's-like axonal dystrophy. J Neurosci. 2011; 31:7817–7830. [PubMed: 21613495]

Lynch-Day MA, Mao K, Wang K, Zhao M, Klionsky DJ. The role of autophagy in Parkinson's disease. Cold Spring Harbor perspectives in medicine. 2012; 2:a009357. [PubMed: 22474616]

Maday S, Wallace KE, Holzbaur EL. Autophagosomes initiate distally and mature during transport toward the cell soma in primary neurons. J Cell Biol. 2012; 196:407–417. [PubMed: 22331844]

Mann SS, Hammarback JA. Molecular characterization of light chain 3. A microtubule binding subunit of MAP1A and MAP1B. J Biol Chem. 1994; 269:11492–11497. [PubMed: 7908909]

Martinez-Vicente M, Talloczy Z, Wong E, Tang G, Koga H, Kaushik S, de Vries R, Arias E, Harris S, Sulzer D, et al. Cargo recognition failure is responsible for inefficient autophagy in Huntington's disease. Nat Neurosci. 2010; 13:567–576. [PubMed: 20383138]

Mizushima N, Yamamoto A, Matsui M, Yoshimori T, Ohsumi Y. In vivo analysis of autophagy in response to nutrient starvation using transgenic mice expressing a fluorescent autophagosome marker. Mol Biol Cell. 2004; 15:1101–1111. [PubMed: 14699058]

Morris RL, Hollenbeck PJ. The regulation of bidirectional mitochondrial transport is coordinated with axonal outgrowth. J Cell Sci. 1993; 104(Pt 3):917–927. [PubMed: 8314882]

Moughamian AJ, Holzbaur EL. Dynactin is required for transport initiation from the distal axon. Neuron. 2012; 74:331–343. [PubMed: 22542186]

Muresan Z, Muresan V. Coordinated transport of phosphorylated amyloid-beta precursor protein and c-Jun NH2-terminal kinase-interacting protein-1. J Cell Biol. 2005; 171:615–625. [PubMed: 16301330]

Narendra D, Tanaka A, Suen DF, Youle RJ. Parkin is recruited selectively to impaired mitochondria and promotes their autophagy. J Cell Biol. 2008; 183:795–803. [PubMed: 19029340]

Nihalani D, Wong HN, Holzman LB. Recruitment of JNK to JIP1 and JNK-dependent JIP1 phosphorylation regulates JNK module dynamics and activation. J Biol Chem. 2003; 278:28694–28702. [PubMed: 12756254]

Noda NN, Kumeta H, Nakatogawa H, Satoo K, Adachi W, Ishii J, Fujioka Y, Ohsumi Y, Inagaki F. Structural basis of target recognition by Atg8/LC3 during selective autophagy. Genes to cells : devoted to molecular & cellular mechanisms. 2008; 13:1211–1218. [PubMed: 19021777]

Pankiv S, Alemu EA, Brech A, Bruun JA, Lamark T, Overvatn A, Bjorkoy G, Johansen T. FYCO1 is a Rab7 effector that binds to LC3 and PI3P to mediate microtubule plus end-directed vesicle transport. J Cell Biol. 2010; 188:253–269. [PubMed: 20100911]

Perlson E, Jeong GB, Ross JL, Dixit R, Wallace KE, Kalb RG, Holzbaur EL. A switch in retrograde signaling from survival to stress in rapid-onset neurodegeneration. J Neurosci. 2009; 29:9903–9917. [PubMed: 19657041]

Rai AK, Rai A, Ramaiya AJ, Jha R, Mallik R. Molecular adaptations allow dynein to generate large collective forces inside cells. Cell. 2013; 152:172–182. [PubMed: 23332753]

Ravikumar B, Acevedo-Arozena A, Imarisio S, Berger Z, Vacher C, O'Kane CJ, Brown SD, Rubinsztein DC. Dynein mutations impair autophagic clearance of aggregate-prone proteins. Nat Genet. 2005; 37:771–776. [PubMed: 15980862]

Rogov VV, Suzuki H, Fiskin E, Wild P, Kniss A, Rozenknop A, Kato R, Kawasaki M, McEwan DG, Lohr F, et al. Structural basis for phosphorylation-triggered autophagic clearance of Salmonella. The Biochemical journal. 2013; 454:459–466. [PubMed: 23805866]

Rubino E, Rainero I, Chio A, Rogaeva E, Galimberti D, Fenoglio P, Grinberg Y, Isaia G, Calvo A, Gentile S, et al. SQSTM1 mutations in frontotemporal lobar degeneration and amyotrophic lateral sclerosis. Neurology. 2012; 79:1556–1562. [PubMed: 22972638]

Stokin GB, Lillo C, Falzone TL, Brusch RG, Rockenstein E, Mount SL, Raman R, Davies P, Masliah E, Williams DS, et al. Axonopathy and transport deficits early in the pathogenesis of Alzheimer's disease. Science. 2005; 307:1282–1288. [PubMed: 15731448]

Stromhaug PE, Berg TO, Fengsrud M, Seglen PO. Purification and characterization of autophagosomes from rat hepatocytes. The Biochemical journal. 1998; 335(Pt 2):217–224. [PubMed: 9761717]

Sugawara K, Suzuki NN, Fujioka Y, Mizushima N, Ohsumi Y, Inagaki F. The crystal structure of microtubule-associated protein light chain 3, a mammalian homologue of Saccharomyces cerevisiae Atg8. Genes to cells : devoted to molecular & cellular mechanisms. 2004; 9:611–618. [PubMed: 15265004]

Sun F, Zhu C, Dixit R, Cavalli V. Sunday Driver/JIP3 binds kinesin heavy chain directly and enhances its motility. EMBO J. 2011; 30:3416–3429. [PubMed: 21750526]

Tumbarello DA, Waxse BJ, Arden SD, Bright NA, Kendrick-Jones J, Buss F. Autophagy receptors link myosin VI to autophagosomes to mediate Tom1-dependent autophagosome maturation and fusion with the lysosome. Nat Cell Biol. 2012; 14:1024–1035. [PubMed: 23023224]

van Niekerk EA, Willis DE, Chang JH, Reumann K, Heise T, Twiss JL. Sumoylation in axons triggers retrograde transport of the RNA-binding protein La. Proc Natl Acad Sci U S A. 2007; 104:12913–12918. [PubMed: 17646655]

Verhey KJ, Meyer D, Deehan R, Blenis J, Schnapp BJ, Rapoport TA, Margolis B. Cargo of kinesin identified as JIP scaffolding proteins and associated signaling molecules. J Cell Biol. 2001; 152:959–970. [PubMed: 11238452]

Wild P, Farhan H, McEwan DG, Wagner S, Rogov VV, Brady NR, Richter B, Korac J, Waidmann O, Choudhary C, et al. Phosphorylation of the autophagy receptor optineurin restricts Salmonella growth. Science. 2011; 333:228–233. [PubMed: 21617041]

Willoughby EA, Perkins GR, Collins MK, Whitmarsh AJ. The JNK-interacting protein-1 scaffold protein targets MAPK phosphatase-7 to dephosphorylate JNK. J Biol Chem. 2003; 278:10731–10736. [PubMed: 12524447]

Wong YC, Holzbaur EL. The Regulation of Autophagosome Dynamics by Huntingtin and HAP1 Is Disrupted by Expression of Mutant Huntingtin, Leading to Defective Cargo Degradation. J Neurosci. 2014; 34:1293–1305. [PubMed: 24453320]

Highlights

- Retrograde axonal transport of autophagosomes requires the scaffolding protein JIP1
- JIP1 binds directly to the autophagosome protein LC3 via a conserved LIR motif
- LC3-binding to JIP1 blocks the JIP1-mediated activation of kinesin-1 motor activity
- JIP1 dephosphorylation by organelle-bound MKP1 may also block kinesin-1 activation

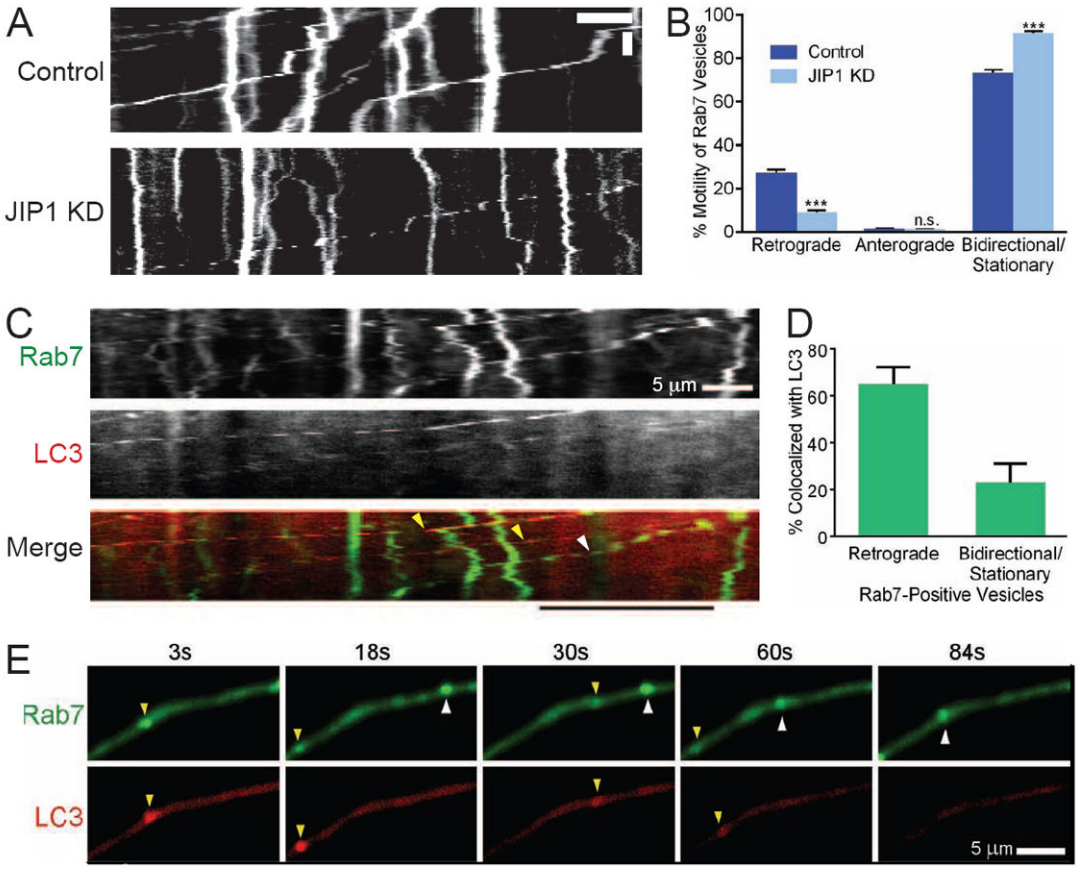

Figure 1. JIP1 Knockdown Disrupts Transport of Rab7-Positive Vesicles

(A) Representative kymographs of EGFP-Rab7-positive late endosome motility in DRGs transfected with JIP1 siRNA. Kymographs represent motion as displacement along the axon (x-axis) over time (y-axis).

(B) JIP1 knockdown significantly decreases the retrograde motility of EGFP-Rab7-positive vesicles and concurrently increases the percentage of bidirectional and stationary Rab7-positive vesicles in DRG axons. Data represents 3 independent experiments (n = 13–16 neurons).

(C) EGFP-Rab7 and mCherry-LC3 co-migrate in the mid-axon of DRGs. Representative kymographs of a 3-minute movie show two retrograde vesicles that are co-positive for EGFP-Rab7 and mCherry-LC3 (yellow arrowheads) and one retrograde vesicle that is only positive for EGFP-Rab7 (white arrowhead). The underlined region is highlighted in Figure 1E with time-lapse images.

(D) The majority of retrograde EGFP-Rab7-positive vesicles co-migrate with mCherry-LC3 while a low percentage of bidirectional/stationary EGFP-Rab7-positive vesicles co-migrate with mCherry-LC3 (n = 7 double-transfected neurons).

(E) Time-lapse images from the underlined region in Figure 1C.

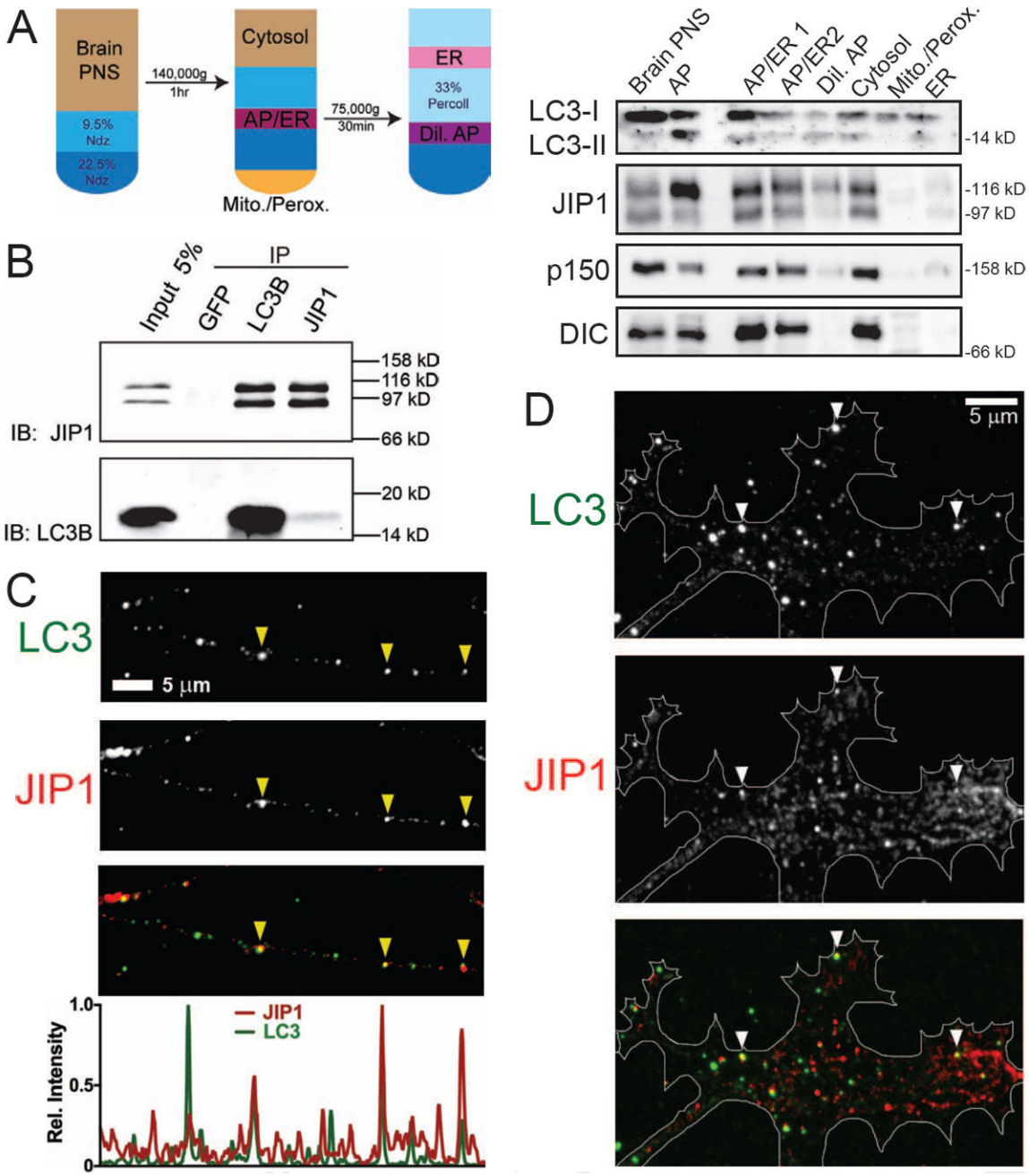

Figure 2. JIP1 Associates with Autophagosomes

(A) High-molecular-weight JIP1 is enriched in purified autophagosomes. The purified autophagosome fraction (AP), which is enriched for lipidated LC3-II, contains components of the retrograde motor complex, including the p150^{Glued} subunit of dynactin and DIC (dynein intermediate chain). Briefly, homogenized brain post-nuclear supernantant (PNS) was subject to Nycodenz gradient centrifugation, which yielded fractions enriched for cytosol, autophagosomes and ER (AP/ER), and mitochondria and peroxisomes (Mito./Perox.). Centrifugation of the AP/ER fraction through a Percoll gradient resulted in separation into an ER fraction and a dilute autophagosome (Dil. AP) fraction, which was

then concentrated in a subsequent spin to yield the autophagosome fraction (AP). Each lane contains equal protein loading. Data represents 2 independent experiments.

(B) Endogenous JIP1 coimmunoprecipitates with LC3 in mouse brain homogenate. A monoclonal anti-LC3 antibody coimmunoprecipitates both 90-kD and 110-kD bands of JIP1. A monoclonal JIP1 antibody also coimmunoprecipitates LC3, though to a lesser extent. Data represents 2 independent experiments.

(C,D) Endogenous JIP1 and LC3 colocalize on vesicles along axons and in distal axon tips of nontransfected DRGs (arrowheads). Representative images from 2 independent experiments show immunofluorescence staining of LC3 (green) and JIP1 (red).

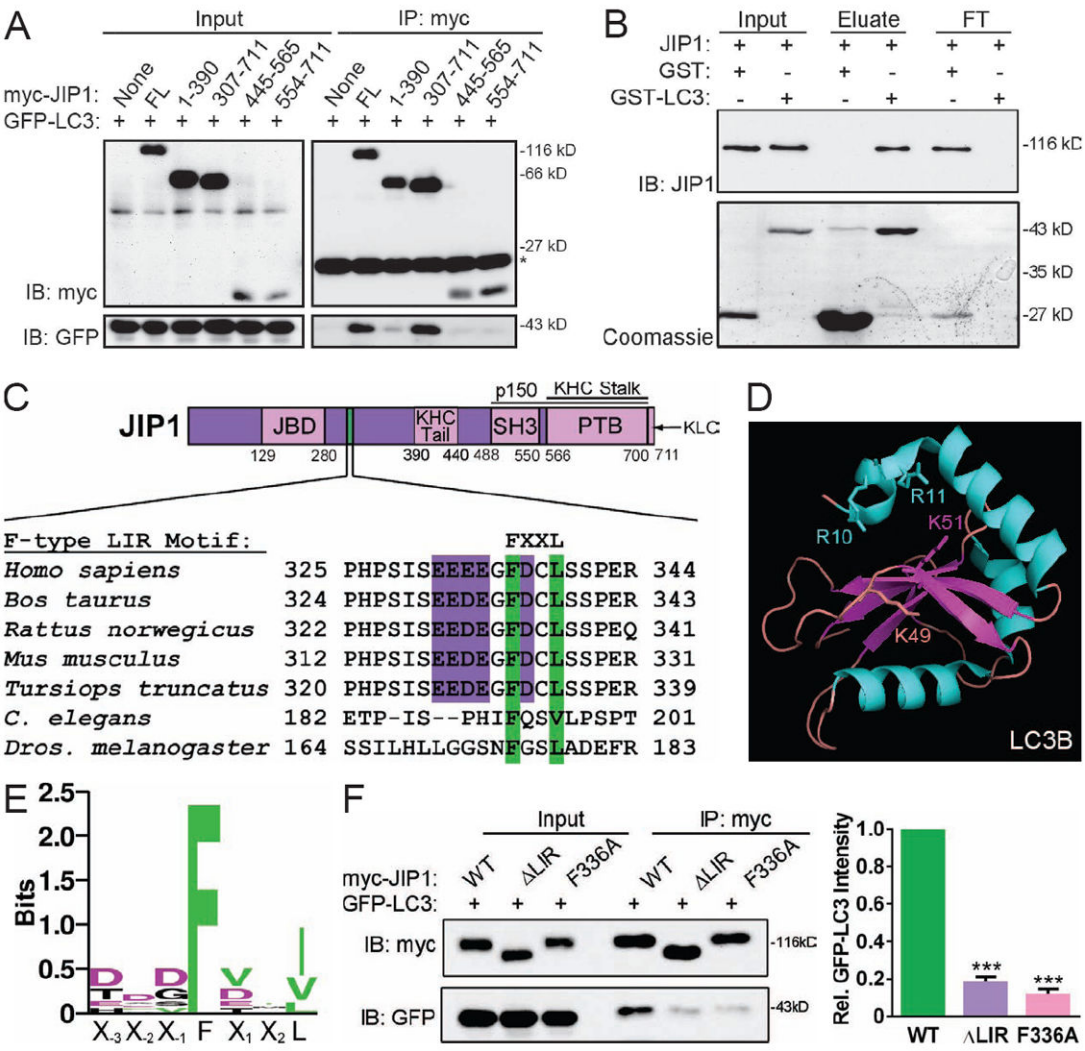

Figure 3. JIP1 Binds to the Autophagosome Adaptor LC3

(A) JIP1 binds to LC3. Lysates from COS7 cells co-transfected with GFP-LC3 and myc-JIP1 fragments were immunoprecipitated with an anti-myc antibody. Both full-length myc-JIP1, myc-JIP1[1-390] and myc-JIP1[307-711] coimmunoprecipitated GFP-LC3. Asterisk denotes antibody light chain.

(B) JIP1 binds directly to GST-LC3. GST control and GST-LC3 bound to glutathione beads were incubated with recombinant untagged JIP1. GST did not bind to JIP1 while GST-LC3 saturated binding of JIP1. The ~43-kD band in the GST eluate lane may represent spillover of protein from the adjacent lane.

(C) JIP1 contains a predicted F-type LIR (LC3-interacting region) motif. This EEEEGFDCL motif is conserved in mammalian JIP1 and contains three components that define LIR motifs and function to mediate binding to LC3 – a central aromatic phenylalanine residue, a leucine residue, and several flanking acidic residues.

(D) Crystal structure of LC3 highlighting LIR-interacting residues. The 2.05-Angstrom crystal structure of rat LC3B-I (PDB code U1GM) (Sugawara et al., 2004) was visualized using the PyMOL PDB viewer. Sticks highlight key residues in the hydrophobic pockets of

LC3 (K49, K51) that interact with the LIR aromatic residue and leucine as well as the basic residues in N-terminal LC3 (R10, R11) that interact with the acidic residues preceding the LIR aromatic residue.

(E) Sequence logo of several F-type LIR motifs shows the degree of conservation at each residue. The net height of letters indicates the degree of conservation at each position while the heights of individual letters indicates that relative frequency of certain residues at each position. F-type LIR motifs of JIP1, optineurin, FYCO1, ULK1, ATG13, FIP200, and TBC1D5 (Birgisdottir et al., 2013) were plotted using the WebLogo server (http://weblogo.berkeley.edu/logo.cgi).

(F) Truncation or mutation of LIR decreases JIP1 binding to LC3. Mutant myc-JIP1-ΔLIR lacks AA327-341 (PSISEEEEGFDCLSS). Lysates from COS7 cells co-transfected with GFP-LC3 and either wildtype or mutant myc-JIP1 were immunoprecipitated with an anti-myc antibody. Densitometry of coimmunoprecipitated GFP-LC3 bands shows that lysates from cells expressing myc-JIP1-ΔLIR or myc-JIP1-F336A have ~20% of the GFP-LC3 binding ability of wildtype myc-JIP1.

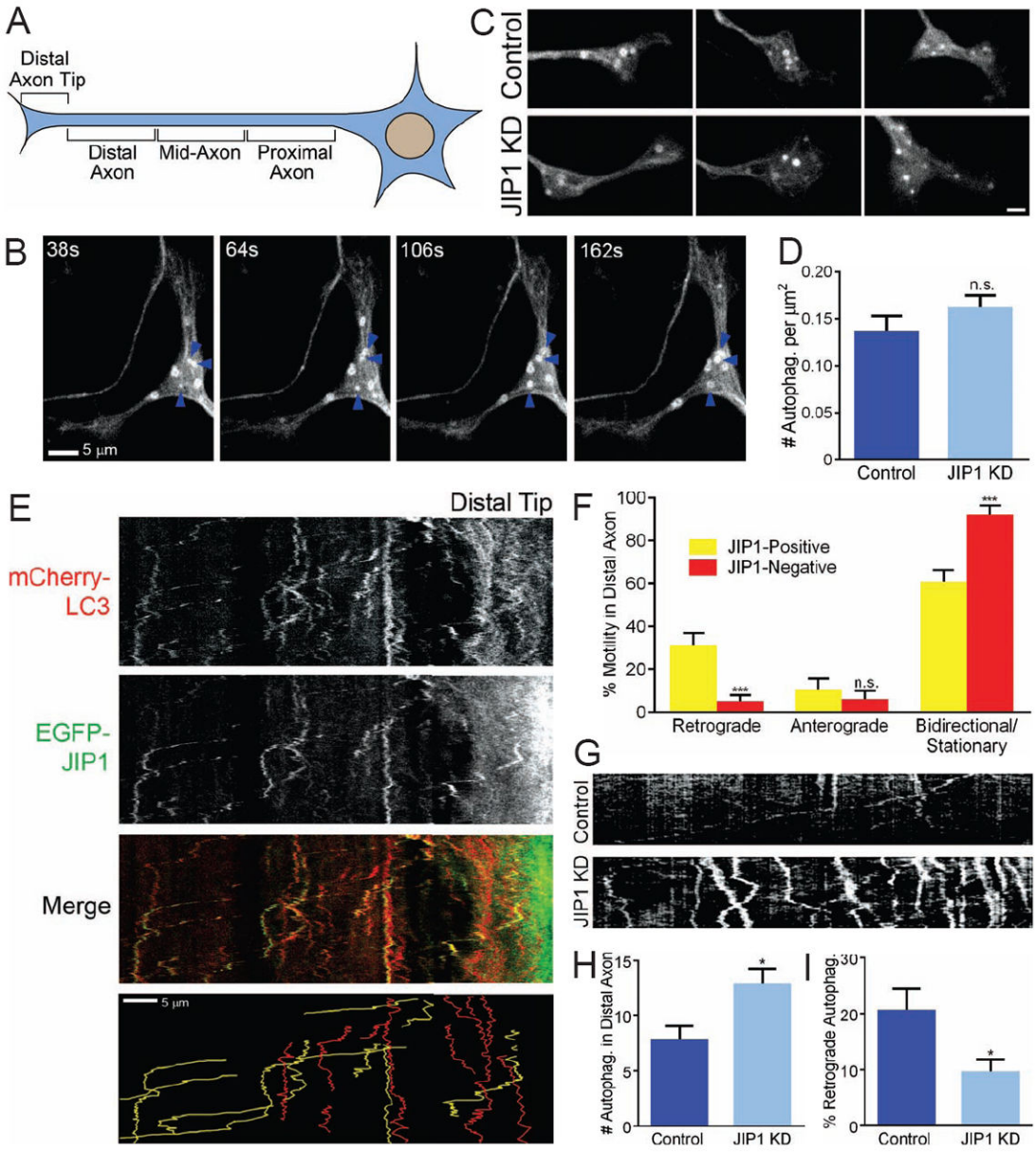

Figure 4. Efficient Exit of Autophagosomes from the Distal Axon Requires JIP1

(A) Schematic of four distinct axonal regions: the distal axon tip, the distal axon, the mid-axon, and the proximal axon.

(B) Representative time-lapse confocal images highlight autophagosome biogenesis in the distal axon tip of a DRG cultured from the GFP-LC3 mouse and transfected with fluorescent JIP1 siRNA. Newly formed autophagosomes are small punctate structures that gradually enlarge into a ring-like structure (arrowheads) on the timescale of 2–3 minutes.

(C-D) JIP1 knockdown does not perturb the number of autophagosomes in the distal axon tip. The density of autophagosomes in GFP-LC3 DRGs transfected with fluorescent JIP1 siRNA did not differ significantly from control neurons ($p = 0.23$). Data represents 3 independent experiments ($n = 18–22$ neurons).

(E) Retrograde mCherry-LC3 autophagosomes selectively co-migrate with EGFP-JIP1 in the distal axon. Wildtype DRGs were co-transfected with mCherry-LC3 and EGFP-JIP1. Representative kymographs were generated from a 10-minute movie and pseudo-colored traces of mCherry-LC3 motility (bottom panel) highlight EGFP-JIP1-positive (yellow) and EGFP-JIP1-negative (red) autophagosomes.

(F) A greater percentage of EGFP-JIP1-positive autophagosomes than EGFP-JIP1-negative autophagosomes move in the retrograde direction in the distal axon. For each neuron, mCherry-LC3-positive autophagosomes were binned as JIP1-positive or JIP1-negative and separately analyzed for direction of transport. Data represents 3 independent experiments (n = 5 neurons, 19–29 autophagosomes).

(G) Representative kymographs of GFP-LC3 motility in the distal axon of DRGs transfected with fluorescent JIP1 siRNA. Data from Figures 5C–5E represent data from 3 independent experiments (n = 11–12 neurons).

(H) The mean number of GFP-LC3 autophagosomes in the distal axon increases upon JIP1 knockdown.

(I) The percentage of retrograde GFP-LC3 autophagosomes in the distal axon decreases upon JIP1 knockdown.

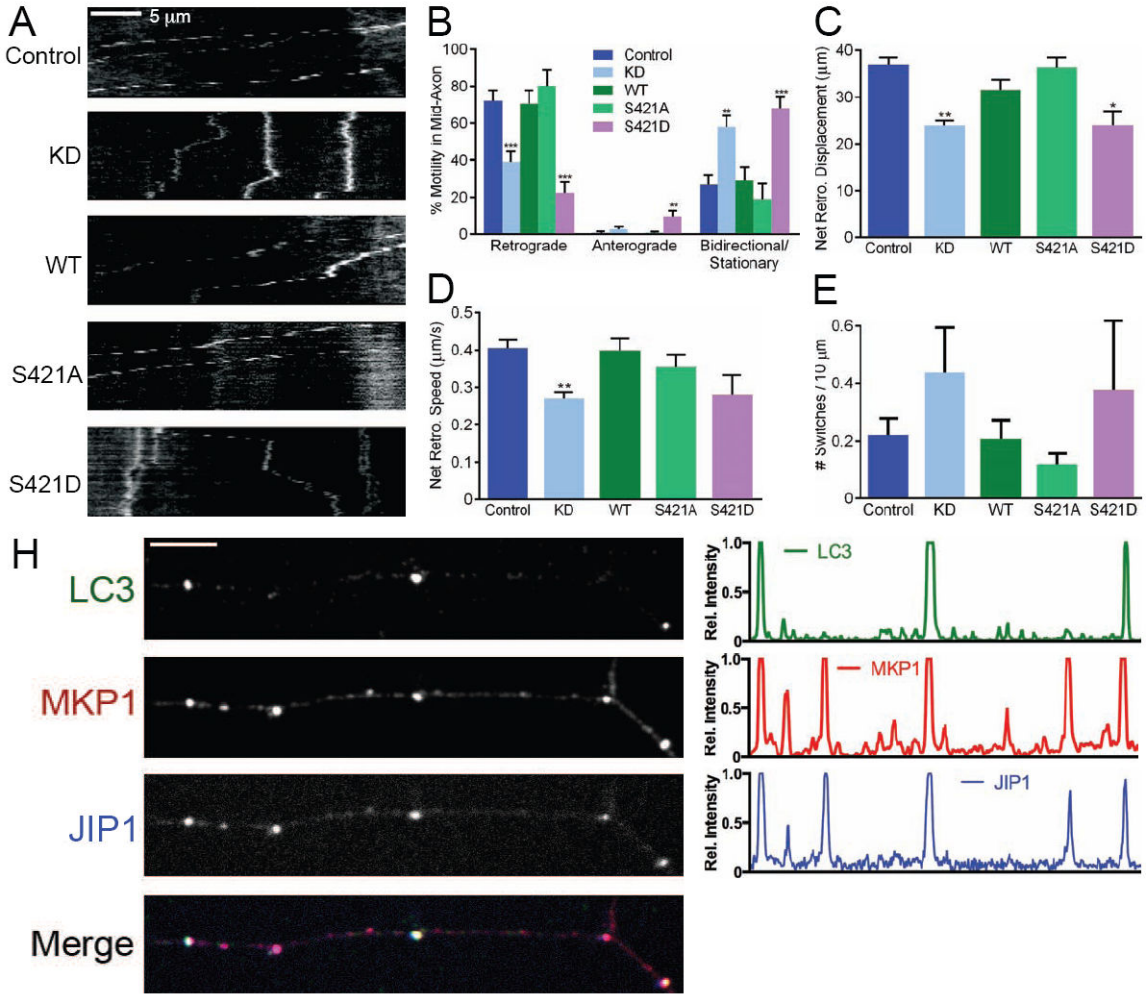

Figure 5. Processive Retrograde Autophagosome Transport in the Mid-Axon Requires Nonphosphorylated JIP1

(A) Representative 3-minute kymographs of GFP-LC3 autophagosome motility in DRGs transfected with red fluorescent siRNA targeted to mouse JIP1 and rescued with a bidirectional construct co-expressing resistant human wildtype or mutant JIP1 (S421A or S421D) and the transfection marker BFP.

(B) JIP1 knockdown significantly decreased the percentage of retrograde autophagosomes and increased the percentage of bidirectional/stationary autophagosomes. Both wildtype human JIP1 and phosphodeficient JIP1-S421A restore retrograde autophagosome transport, but phosphomimetic JIP1-S421D cannot restore the percentage of retrograde autophagosomes and instead increases the percentage of anterograde autophagosomes. Data in Figs. 5B–5E represent 3 independent experiments (n = 7–16 neurons).

(C) JIP1 knockdown decreased the net displacement of retrograde autophagosomes. Rescue with the S421A mutant restored net retrograde displacement while expression of the S421D mutant decreased net retrograde displacement.

(D) JIP1 knockdown decreased the net speed of retrograde autophagosomes. Rescue with the S421A mutant restored net retrograde speed.

(E) Quantification of the frequency of directional switches in the mid-axon of DRGs. Absolute numbers of directional switches were quantified for individual retrograde autophagosomes and normalized against the net displacement. Note that these trends are not statistically significant.

(F) Endogenous JIP1 and MKP1 colocalize on autophagosomes along the axon. Representative images and linescans of nontransfected DRG neurons immunostained with a mouse monoclonal antibody against LC3 (green), a rabbit antibody against MKP1 (red), and a sheep monoclonal antibody against JIP1 (blue). Scale bar = 5 μm.

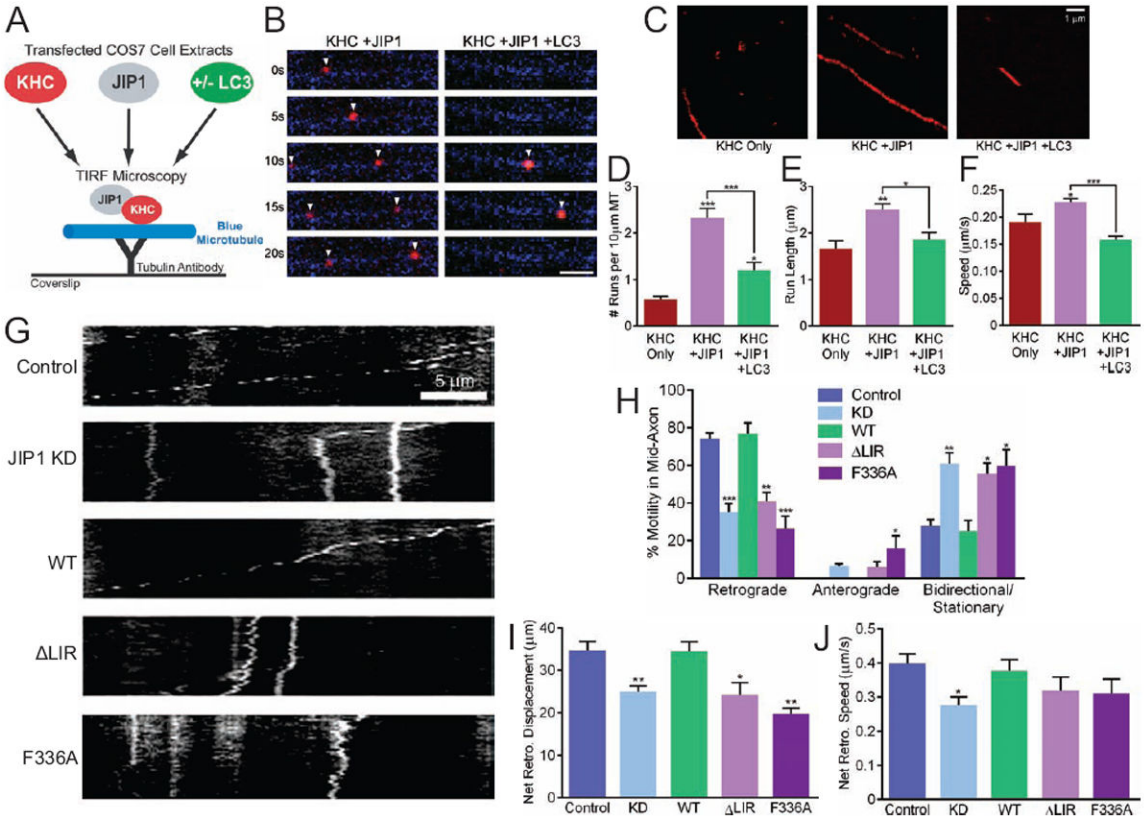

Figure 6. LC3 Binding to JIP1 Blocks Activation of Kinesin *in vitro* and is Necessary for Retrograde Transport of Autophagosomes in the Mid-Axon

(A) Schematic of *in vitro* TIRF motility assays. COS7 cells transfected with KHC-Halo were incubated with membrane-permeable red TMR-conjugated HaloTag ligand. This lysate from KHC-Halo-expressing cells was combined with lysate from myc-JIP1-expressing cells and applied to flow chambers containing blue AMCA-labeled fluorescent microtubules, which were immobilized on glass coverslips with an anti-tubulin antibody.

(B) Time-lapse images acquired from a flow chamber containing KHC-Halo (red) and myc-JIP1 lysates show a motile binding event (arrowheads, left panel) to a microtubule (blue). Images from a chamber containing KHC-Halo, myc-JIP1, and GFP-LC3 lysates show a shorter run (arrowheads, right panel).

(C) Activation of KHC-Halo by JIP1 is abrogated upon addition of LC3. Each representative kymograph shows 100 total frames (~33 seconds).

(D–F) Addition of LC3 decreases the run frequency, run length, and speed of KHC-Halo in the presence of JIP1. The absolute number of runs was normalized to the length of each microtubule. Data from Figs. 6D–6F represent 3 independent experiments (n = 77–99 microtubules, 74–214 runs) and statistical comparisons were made to the KHC-Halo alone condition unless otherwise indicated.

(G) Representative 3-minute kymographs of GFP-LC3 autophagosome motility in DRGs transfected with siRNA targeted to mouse JIP1 and rescued with a bidirectional construct co-expressing resistant human wildtype JIP1 or mutant JIP1-ΔLIR/F336A as well as the fluorescent transfection marker BFP.

(H) DRGs expressing the JIP1-ΔLIR or F336A mutant display decreased percentage of retrograde autophagosomes when compared to control neurons. Data in Figures 6G–6J represent 3 independent experiments (n = 9–13 neurons); statistical comparisons were made against the control condition.

(I) Retrograde autophagosomes in DRGs expressing the JIP1-ΔLIR or F336A mutant display decreased net retrograde displacement.

(J) No statistically significant changes in net retrograde speed of autophagosomes from DRGs expressing JIP1 LIR mutants were observed.

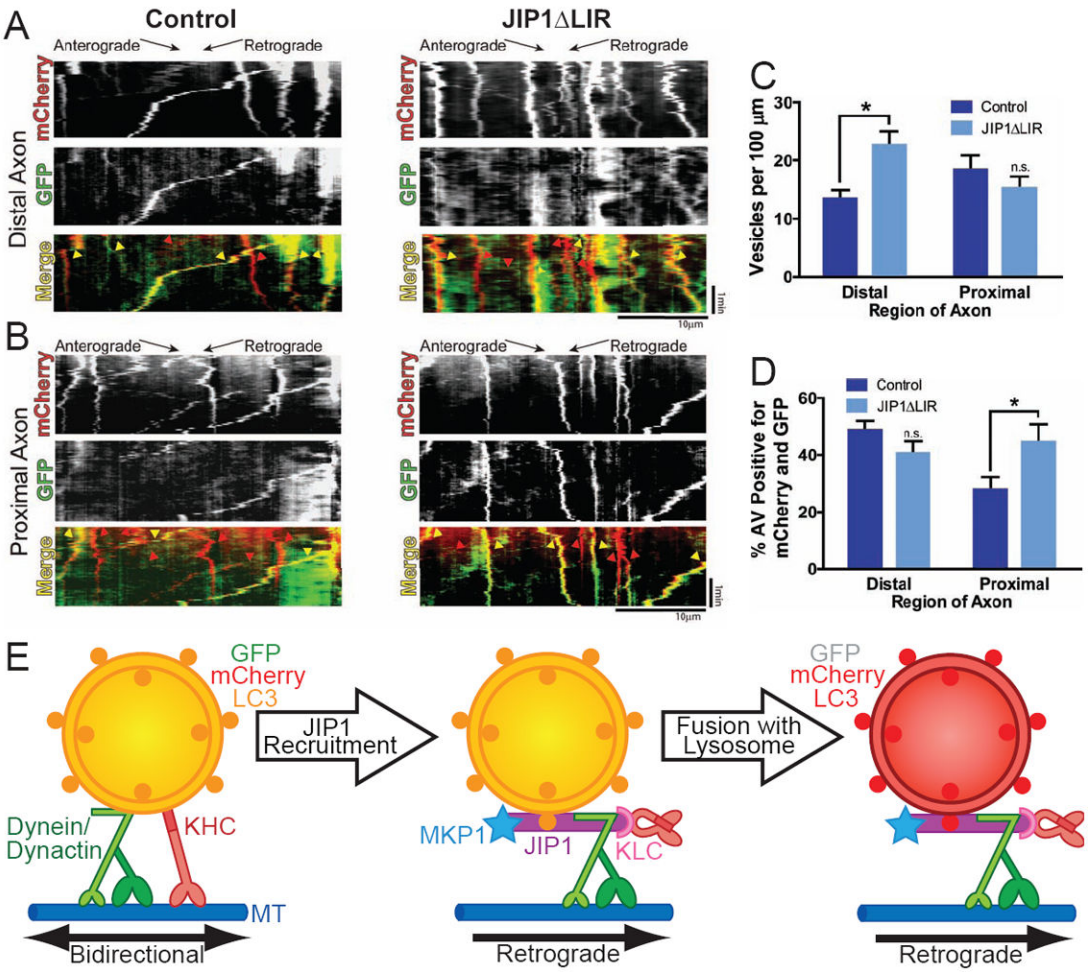

Figure 7. JIP1 Binding to LC3 is Necessary for Autophagosome Acidification in the Proximal Axon

(A,B) Representative kymographs of mCherry-GFP-LC3 motility in the distal and proximal axon of DRGs knocked down and rescued with JIP1-ΔLIR. Data from Figures 7A–7D represent 3 independent experiments (n = 10–12 neurons).

(C) Total number of autophagosomes in the distal axon increases in JIP1-ΔLIR-expressing DRGs. Data from Figures 7C and 7D were analyzed with t-tests comparing wildtype versus mutant neurons from each axonal region and thus are plotted on discontinuous x-axes.

(D) The percentage of immature mCherry- and GFP-positive autophagosomes increases in the proximal axon of JIP1-ΔLIR-expressing DRGs.

(E) Model for the effect of JIP1 recruitment on autophagosome motility and lysosomal fusion. The majority of autophagosomes in the distal axon move in a bidirectional or stationary manner (left). Upon JIP1 recruitment via binding to LC3, autophagosomes begin to exit out of the distal axon and continue into the mid-axon and the proximal (middle). Because LC3 binding to JIP1 reduces the ability of JIP1 to activate kinesin, JIP1 remains bound to $p150^{Glued}$ and sustains retrograde autophagosome transport in the mid-axon. Robust retrograde autophagosome transport is important for fusion with lysosomes and efficient cargo degradation.